

# Unsteady Numerical Investigation Strategy of Natural Convection in an Isosceles Superimposed Triangular Enclosure

Elhadj BENACHOUR\*, Khadidja ASNOUNE\*\*, Mohamed HASNAT\*\*\*, Belkacem DRAOUI\*\*\*\*

\*ENERGARID Laboratory, Faculty of Science and Technology University of TAHRI MOHAMED, Bechar, Algeria, E-mail: benachour.elhadj@univ-bechar.dz

\*\*Tahri Mohamed University of Bechar, Smart Grids Laboratory, B.P 417, 08000, Bechar, Algeria, E-mail: kh\_asnoune@yahoo.fr

\*\*\*ENERGARID Laboratory, Faculty of Science and Technology University of TAHRI MOHAMED, Bechar, Algeria, E-mail: hasnat.mohamed@univ-bechar.dz

\*\*\*\*ENERGARID Laboratory, Faculty of Science and Technology University of TAHRI MOHAMED, Bechar, Algeria, E-mail: draoui.belkacem@univ-bechar.dz

<https://doi.org/10.5755/j02.mech.34030>

## 1. Introduction

In modern fluid mechanics engineering and research fields like temperature and stress [1], heat transfer [2], mass transfer [3], and practical approach [4], numerical flow simulation is an essential component. This is accomplished by using a variety of software with varying degrees of efficiency for edge computing and cloud manufacturing applications for technological process monitoring based on digital twins [5]. Accordingly, it was possible to simulate a flexible structure dynamically using MATLAB [6] and other software like COMSOL [7, 8], ANSYS [9, 10] and Fluent [11]. Obtaining high heat transfer rates through various enhancement techniques can lead to substantial energy savings. Turbulence promoters in heat exchangers primarily enhance heat transfer operations by offering optimal flow conditions with varying geometrical characteristics and diverse directions.

The process of heat transfer is strongly related to the performance of the sizes and directions effects of the geometries. Analysing how heat moves through packets because of its various uses in the field of applied engineering, natural convection has garnered the attention of scientists [12]. The design for high-performance density electronics using effective cooling techniques is necessary for dependable operation. There are numerous ways for electronic devices to fail.

Thermal effects are strongly related to processes such as void formation, metal migration, and intermetallic growth [13]. Despite the diversity of uses and their complexity, because a conducting fluid is used in the process of creating materials for industrial problems and microelectronic heat transfer devices that is occasionally subjected to the convection mode of heat transfer, natural convection flows have received a lot of attention. In this instance, a Lorentz force that impacts the rate of heat transfer causes the fluid to have decreased flow velocities [14]. There is a wealth of literature on the heating and cooling of different geometrical enclosure shapes, including squares, rectangles, trapezoids, quadrants, etc., from the enclosure walls [15-21]. The solution of natural convection equations has been extensively examined in right-angle triangular enclosures and extensively examined in past research [22-27]. Nevertheless, natural convection in isosceles triangle enclosures hasn't been studied much. Many residential and

commercial applications heavily rely on energy transfer analysis in triangle-shaped enclosure heated from the side or below [28-33], like heat transfer through the roof Buildings, swimming pools, dough mixer and ice cream and juice cooler. Additional flow-related phenomena have been discussed in [34-36] among other places. In this study, a triangle's inherent convection combined with momentary convection in an isosceles-superimposed triangular enclosure is suggested as a solution for natural convection heat transfer difficulties in a steady state, such as free convection in an equilateral triangle cavity. Where the small triangle contains water and the big triangle contains air. It is a technique of cooling or heating water by air, that can be found in the automobile industry generally or the generators. This study describes the impact of baffle length, aspect ratio, and Rayleigh number on flow field and heat transfer. The length of the baffle or interrupter is proven to have a significant impact on heat transfer. Temperature contours and stream functions are used to display the results.

The Nusselt number is used to represent the heat transfer. The constant flow behavior that results from heating an isothermal, quiescent Newtonian fluid of air by the water is examined in a two-dimensional triangular enclosure of height  $H = 0.86$ ,  $L = 3f$ ,  $f = 2g$ ,  $g = 0.1$ ,  $a = 5g$ ,  $d = a$ ,  $h = 5g$ , and horizontal length equal to  $L+2f$ . The top

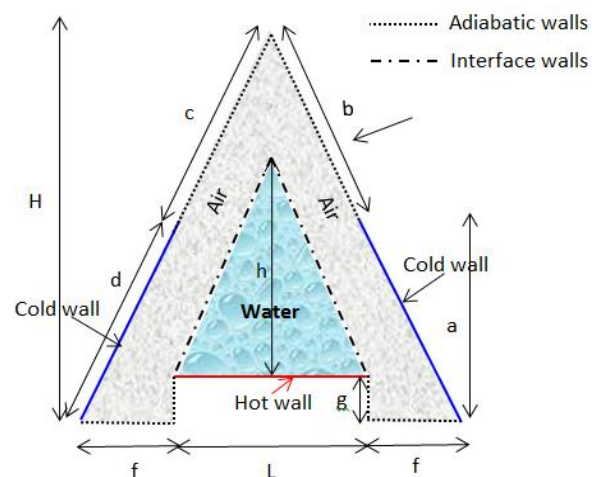


Fig. 1 Schematic approach

tip of the container has a flow interrupter fastened to it. As illustrated in Fig. 1, the bottom base is heated, the left and right sloped surfaces are cooled, and all other walls are adiabatic.

The objectives of this study are:

- study of heat transfer by convection in an isosceles superimposed triangular enclosure;
- control the heat exchange between two different liquids;
- study the heating of the air by the water.

## 2. Mathematical model

The Boussinesq approximation is followed and the fluid is considered to be incompressible, where  $g$  is the gravity and the system's coefficient of thermal expansion is  $\beta$ . In these situations, the equations controlling the flow and energy as well as continuity in two dimensions are provided respectively by the equation of Continuity, X-momentum, Y-momentum and Energy using physical parameters ( $\mu$ ,  $\nu$ ,  $P$  and  $T$ ):

$$\frac{\partial \mu}{\partial X} + \frac{\partial \nu}{\partial Y} = 0, \quad (1)$$

$$\frac{\partial \mu}{\partial t} + \mu \frac{\partial \mu}{\partial X} + \nu \frac{\partial \mu}{\partial Y} = -\frac{1}{\rho} \frac{\partial P}{\partial X} + \nu \nabla^2 \mu, \quad (2)$$

$$\frac{\partial \nu}{\partial t} + \mu \frac{\partial \nu}{\partial X} + \nu \frac{\partial \nu}{\partial Y} = -\frac{1}{\rho} \frac{\partial P}{\partial Y} + \nu \nabla^2 \nu + g\beta \frac{\partial T}{\partial Y}, \quad (3)$$

$$\frac{\partial T}{\partial t} + \mu \frac{\partial T}{\partial X} + \nu \frac{\partial T}{\partial Y} = \frac{K}{\rho C_p} \nabla^2 T. \quad (4)$$

Here:  $\rho$ ,  $\nu$ ,  $C_p$  and  $K$  respectively represent the density, kinematic viscosity, specific heat and thermal conductivity of the thermal physical properties of fluid.

The dimensionless variables in the equations that are utilized to formulate the stream function and write Helmholtz in terms of vorticity ( $\psi^*$ ,  $\omega^*$ ) are as follows:

$$\begin{aligned} \frac{\partial \omega^*}{\partial t} + \frac{\partial \psi^*}{\partial y} \frac{\partial \omega^*}{\partial x} - \frac{\partial \psi^*}{\partial x} \frac{\partial \omega^*}{\partial y} &= \\ = Pr \nabla^2 \omega^* + Ra Pr \frac{\partial \bar{T}}{\partial x}, \end{aligned} \quad (5)$$

where:  $Ra$  and  $Pr$  are respectively the dimensionless flow numbers Rayleigh and Prandtl

$$\frac{\partial \bar{T}}{\partial t} + \frac{\partial \psi^*}{\partial y} \frac{\partial \bar{T}}{\partial x} - \frac{\partial \psi^*}{\partial x} \frac{\partial \bar{T}}{\partial y} = \frac{\partial^2 \bar{T}}{\partial x^2} + \frac{\partial^2 \bar{T}}{\partial y^2}, \quad (6)$$

$$\frac{\partial^2 \psi}{\partial X^2} + \frac{\partial^2 \psi}{\partial Y^2} = -\omega, \quad (7)$$

$$\mu = \frac{\partial \psi}{\partial Y}, \quad \nu = -\frac{\partial \psi}{\partial X}, \quad \omega = \frac{\partial \nu}{\partial X} - \frac{\partial \mu}{\partial Y}. \quad (8)$$

Here, dimensionless variables in the equations above are defined by:

$$\begin{cases} \bar{x} = \frac{X}{L}, \quad \bar{y} = \frac{Y}{L}, \quad \psi^* = \frac{\psi}{a}, \\ \omega^* = \frac{\omega}{a/L^2}, \quad -\omega^* = \frac{\partial^2 \psi^*}{\partial \bar{x}^2} + \frac{\partial^2 \psi^*}{\partial \bar{y}^2}, \\ \bar{P} = \frac{P}{\rho \mu^2}, \quad \bar{T} = \frac{T - T_i}{T_c - T_i}, \quad \bar{t} = \frac{t}{L^2/a}. \end{cases} \quad (9)$$

## 3. Procedure of simulation

First, the CFD Software is used to perform the numerical calculation. The finite volume numerical method was applied in this paper. The related algebraic equations entail the functions discretized using the finite difference method and integrated using the finite volume approach utilized in the CFD code were compared in this context and the SIMPLE algorithm [34] was selected.

The schema Quick is used to evaluate the convective terms in each equation. The time term is discretized using an entirely implicit technique. When the highest relative change of all variables ( $\psi^*$ ,  $\omega^*$  and  $\bar{T}$ ) between two successive times is not less than 1.e4, the solution is said to have obtained convergence. To effectively monitor any changes in the thermal and hydrodynamic fields, we employed a non-stationary grid consisting of 3837 nodes and 7672 elements. Table 1 provides the thermophysical properties of basic fluids.

Table 1

Base fluids Thermo physical properties

Physical properties	Air	Water Liquid
Density, kg/m <sup>3</sup>	1.220	998.2
$C_p$ , J/kg-K	1006.430	4182.0
$\lambda$ , W/m-K	0.02420	0.6
Viscosity, kg/m-s	1.78940e-05	0.001003

The pressure produced by air movement can be exploited to measure the conditions of the air and water. For its part, the air's density depends on the temperature and local atmospheric pressure, which are respectively provided as  $T = 20^\circ\text{C}$  and  $P_{am} = 101.3250$  Pa, under normal atmospheric pressure

## 4. Result and discussion

The boundary constraints have been set up to model a geometric arrangement commonly employed in two-dimensional approximation.

This section covers the flow structure, temperature field, and heat transmission via the hot wall.

The primary objective of this study is to examine and analyze the fluid's thermal and dynamic behavior inside the triangular hollow

### 4.1. Isotherms

Fig. 2 shows the dimensionless temperature profiles at  $y = 0.21$ ; we note that the maximum temperature is at the level of the water fluid for different Rayleigh number  $Ra = 10^3$ ,  $Ra = 10^4$ ,  $Ra = 10^6$ ,  $Ra = 10^7$  and  $Ra = 10^8$ .

Fig. 3 shows the isotherms. The triangular cavity's heat distribution is consistent with the fluid movement

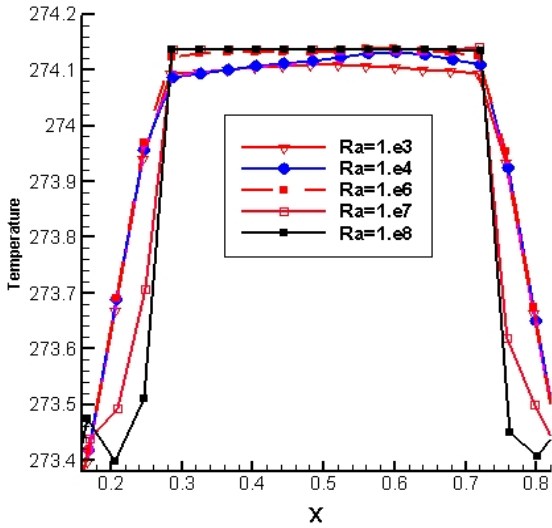


Fig. 2 Dimensionless temperature profiles along the horizontal distance at  $y = 0.21$  and for different Rayleigh number  $Ra = 10^3$ ,  $Ra = 10^4$ ,  $Ra = 10^6$ ,  $Ra = 10^7$  and  $Ra = 10^8$

exhibited by the iso-currents. In fact, for varying numbers of Rayleigh from  $Ra=10^3$  to  $Ra=10^8$ , if the heat distribution in the first triangular cavity shifts, we identify a heating fluid from the interface (see figure), and then in the second triangular cavity. When the  $Pr$  number is fixed at 0.71 for air-fluid and 7.07 for water-fluid, natural convection expands and becomes more prevalent in the first triangular cavity and the second triangular enclosure as a result of the gradual increase in the Rayleigh number, which also causes the isotherms to become more wavy and the heat transfer to increase.

#### 4.2. Streamlines

This section clarifies the streamlines for the triangular cavity for various Rayleigh numbers as displayed in Fig. 4. It is well known that as the Rayleigh number increases, so does the fluid's temperature gradient. As the temperature gradient increases, a large buoyancy force builds up inside the cavity, dramatically altering the fluid's flow pattern. It is noted from streamlines that the two vortices at  $Ra = 10^3$  in Two identical whirlpools are present inside the huge triangle at  $Ra = (10^4 - 10^8)$ . The phenomenon of energy transfer is reproduced for a larger Riley number, but the sizes and speeds are different.

#### 4.3. Local and Average Nusselt numbers

Fig. 5 shows the local Nusselt number profiles, for  $Ra = 10^3 - 10^8$ . The diagram indicates that convective heating starts on the left side and then significantly decreases in the center. The average variation of the Nusselt number as a function of the Rayleigh number is shown in Fig. 6, which shows that convection is the main mode of heat transport, which rises with increasing Rayleigh numbers, and that energy transfer increases as the Rayleigh number increases. Additionally, at low Rayleigh numbers ( $Ra = 10^3$ ), the average Nusselt number is minimal. This is because convection behavior is substantially intensified when the Rayleigh number grows.

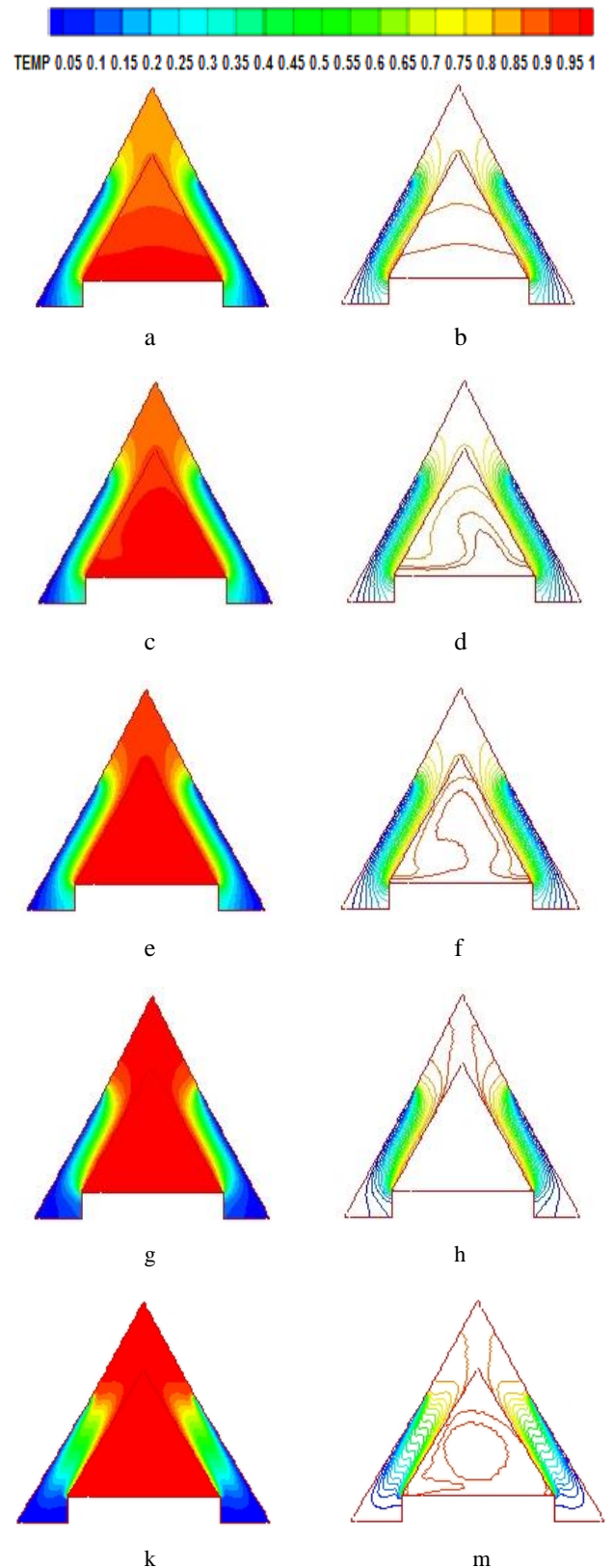


Fig. 3 Isotherms for various Rayleigh number: a -  $Ra = 10^3$ , b -  $Ra = 10^3$ , c -  $Ra = 10^4$ , d -  $Ra = 10^4$ , e -  $Ra = 10^5$ , f -  $Ra = 10^5$ , g -  $Ra = 10^6$ , h -  $Ra = 10^6$ , k -  $Ra = 10^7$ , m -  $Ra = 10^7$  successively

### 5. Comparative study on the influence of geometric shape on flow

The main difference in fluid flow in square shape, round, and triangular cavities are the presence of corners.

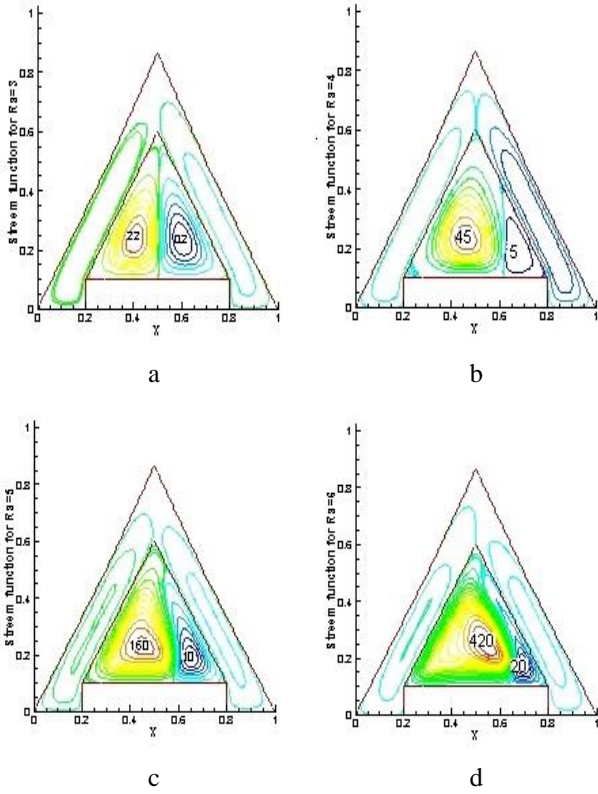


Fig. 4 Differentials of the streamlines for gradually higher Rayleigh numbers successively: a -  $Ra = 10^3$ , b -  $Ra = 10^4$ , c -  $Ra = 10^5$ , d -  $Ra = 10^6$  successively

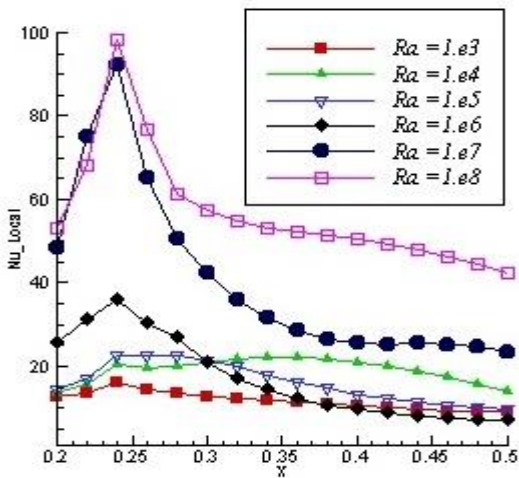


Fig. 5 Profiles of local Nusselt number,  $Ra = 10^3 - 10^8$

Square and triangular cavities have sharp corners, while round cavities have no corners. This difference in geometry leads to different flow patterns and velocity distributions. Vortices in the corners of a square cavity indicate the existence of fluid flow. The boundary layer splitting at the acute corners creates these vortices. The vortices recirculate the fluid within the cavity, which reduces the overall flow velocity. In a round cavity, the fluid flow is more uniform and there are no vortices. This is because the round cavity does not have any sharp corners. The fluid flows smoothly around the curved walls of the cavity, resulting in a higher overall flow velocity. In a triangular cavity, the fluid flow is more complex than in a square or round cavity. This is because the triangular cavity has both sharp and curved corners. The sharp corners lead to the

formation of vortices, while the curved corners allow the fluid to flow more smoothly. The complex flow pattern in a triangular cavity can result in both high and low velocity regions. The following Table 2 summarizes the key differences in fluid flow in round, square, and triangular cavities.

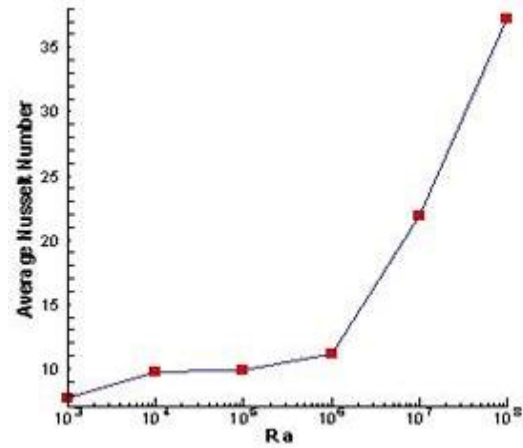


Fig. 6 Average Nusselt number profiles,  $Ra = 10^3 - 10^8$

Table 2  
Comparison of flow rates of triangular enclosures of different shapes

Cavity shape	Corner geometry	Flow pattern	Velocity distribution
Triangular	Sharp and curved corners	Complex flow pattern	Both high and low velocity regions
Round	No angles	Uniform flow	High overall velocity
Square	Sharp corners	Vortices in corners	Reduced overall velocity

## 6. Conclusions

Using ANSYS Fluent for various Rayleigh numbers, the two-dimensional natural convection heat transfer for unstable state conditions in a triangle enclosed and filled with air and another equilateral triangle filled with water as a working fluid has been statistically explored. The results of the study were based on analyzing the effect of many exciting factors, such as the Rayleigh number, where one of the goals was to heat the air with water, that is, to heat a compressible fluid with an incompressible fluid. These provide a significant addition to the analysis the spontaneous convective heat transfer that occurs between two distinct liquids in properties where the following points can be summed up from the current study.

Lower Rayleigh numbers allow for constant compensation of the increased heat transfer rate by lowering the inclination angle below  $45^\circ$ . As the Rayleigh number increases, the flow lines become deformed.

Enclosure in the equilateral triangle shape is crucial for achieving a homogeneous concentration and full-bodied flow.

The slanted angle has a noticeable effect on the flow intensity.

The fluid heats up quickly and significantly faster as the angle of inclination is increased. The fluid of the water core is where convection begins, as experimental study has already shown.

The isosceles triangle enclosure with a reasonably long heat source at the center of the bottom wall exhibits symmetrical flow and temperature fields.

The temperature gradient is a significant factor in this case from a qualitative standpoint. Two integers are multiplied to obtain the Rayleigh number, which quantifies the heat transfer by movement of matter; the higher it is, the more "efficient" the convection. Other dimensionless numbers, such as the Grashof number and the number of Prandtl, are also used to characterize the relative "ease" / "efficiency" of convection and conduction as a mode of heat transfer. The Prandtl number quantifies the relative speed of a medium in transferring energy by movement of matter (convection) or by heat transfer from one step to another (conduction); the higher it is, the more the movements of matter (convection) explain the temperature profiles of the environment. It follows for  $Ra$  that the higher it is, the more convection is favoured. In addition, the study showed that variations in temperature and speed particularly depend on the geometry of the enclosure which becomes increasingly narrow as we move upwards.

#### Acknowledgements

Benachour Elhadj would like to thank all reviewers for taking the time and energy to review our work.

#### References

1. **Prasad, K. V.; Choudhari, R.; Vaidya, H.; Bhat, A.; Animasaun, I. L.** 2023. Analysis of couple stress nanofluid flow under convective condition in the temperature-dependent fluid properties and Lorentz forces, *Heat Transfer* 52: 216-235. <https://doi.org/10.1002/htj.22692>.
2. **Sheikholeslami, M.; Haq, R. U.; Shafee, A.; Li, Z.; Elaraki, Y. G.; Tlili, I.** 2019. Heat transfer simulation of heat storage unit with nanoparticles and fins through a heat exchanger, *International Journal of Heat and Mass Transfer* 135: 470-478. <https://doi.org/10.1016/j.ijheatmasstransfer.2019.02.003>.
3. **Rao, X.; Xin, L.; He, Y.; et al.** 2022. Numerical simulation of two-phase heat and mass transfer in fractured reservoirs based on projection-based embedded discrete fracture model (pEDFM), *Journal of Petroleum Science and Engineering* 208: 109323. <https://doi.org/10.1016/j.petrol.2021.109323>.
4. **DiRenzo, G.V.; Hanks, E.; Miller, D.A.W.** 2023. A practical guide to understanding and validating complex models using data simulations, *Methods in Ecology and Evolution* 14(1): 203-217. <https://doi.org/10.1111/2041-210X.14030>.
5. **Ostaševićius, V.** 2022. Digital Twin-Driven Technological Process Monitoring for Edge Computing and Cloud Manufacturing Applications. In: *Digital Twins in Manufacturing: Virtual and Physical Twins for Advanced Manufacturing* (pp. 267-358). Cham: Springer International Publishing. [https://doi.org/10.1007/978-3-030-98275-1\\_5](https://doi.org/10.1007/978-3-030-98275-1_5).
6. **Giraldo-Londono, O.; Paulino, G. H.** 2021. Poly-Dyna: a Matlab implementation for topology optimization of structures subjected to dynamic loads, *Structural and Multidisciplinary Optimization* 64: 957-990. <https://doi.org/10.1007/s00158-021-02859-6>.
7. **Shi, Y.; Rui, S.; Xu, S.; Wang, N.; Wang, Y.** 2022. COMSOL Modeling of Heat Transfer in SVE Process, *Environments* 9(5), 58. <https://doi.org/10.3390/environments9050058>.
8. **Iqbal, T.; Masood, A.; Khalid, N. R.; Tahir, M. B.; Asiri, A. M.; Alrobei, H.** 2022. Green synthesis of novel lanthanum doped copper oxide nanoparticles for photocatalytic application: correlation between experiment and COMSOL simulation, *Ceramics International* 48(10): 13420-13430. <https://doi.org/10.1016/j.ceramint.2022.01.160>.
9. **Narvydas, E.; Dundulis, R.; Puodziuniene, N.** 2020. Rod end stress analysis for hydraulic cylinder of live floor conveying system, *Mechanika* 26(2): 108-113. <https://doi.org/10.5755/j01.mech.26.2.24675>.
10. **Narvydas, E.; Puodziuniene, N.; Khan Thorappa, A.** 2021. Application of finite element sub-modeling techniques in structural mechanics, *Mechanika* 27(6): 459-464. <https://doi.org/10.5755/j02.mech.25962>.
11. **Tabatabaei Malazi, M.; Eren, E. T.; Luo, J.; Mi, S.; Temir, G.** 2020. Three-dimensional fluid-structure interaction case study on elastic beam, *Journal of Marine Science and Engineering* 8(9), 714. <https://doi.org/10.3390/jmse8090714>.
12. **Triveni, M. K.; Panua, R.** 2016. Numerical simulation of natural convection in a triangular enclosure with caterpillar (C)-curve shape hot wall, *International Journal of Heat and Mass Transfer* 96: 535-547. <https://doi.org/10.1016/j.ijheatmasstransfer.2016.02.002>.
13. **Wankhade, S. D.; Bhor, S. K.; Nagraj, A. M.** 2015. Investigation of thermal performance in natural convection from rectangular interrupted fins—a review, *Intern. J. Innovative Research in Sci. Eng. and Tech.* 4(1): 18528-18535. <https://doi.org/10.15680/IJRSET.2015.0401016>.
14. **Hussein, A. K.; Ashorynejad, H. R.; Sivasankaran, S.; Kolsi, L.; Shikholeslami, M.; Adegun, I. K.** 2016. Modeling of MHD natural convection in a square enclosure having an adiabatic square shaped body using Lattice Boltzmann Method, *Alexandria Engineering Journal* 55(1): 203-214. <https://doi.org/10.1016/j.aej.2015.12.005>.
15. **Pesso, T.; Piva, S.** 2009. Laminar natural convection in a square cavity: low Prandtl numbers and large density differences, *International Journal of Heat and Mass Transfer* 52(3-4): 1036-1043. <https://doi.org/10.1016/j.ijheatmasstransfer.2008.07.005>.
16. **Deng, Q. H.** 2008. Fluid flow and heat transfer characteristics of natural convection in square cavities due to discrete source-sink pairs, *International Journal of Heat and Mass Transfer* 51(25-26): 5949-5957. <https://doi.org/10.1016/j.ijheatmasstransfer.2008.04.062>.
17. **Wu, W.; Ewing, D.; Ching, C. Y.** 2006. The effect of the top and bottom wall temperatures on the laminar natural convection in an air-filled square cavity, *Inter-*

- national Journal of Heat and Mass Transfer 49(11-12): 1999-2008.  
<https://doi.org/10.1016/j.ijheatmasstransfer.2005.11.027>.
18. **Bocu, Z.; Altac, Z.** 2011. Laminar natural convection heat transfer and air flow in three-dimensional rectangular enclosures with pin arrays attached to hot wall, *Applied Thermal Engineering* 31(16): 3189-3195.  
<https://doi.org/10.1016/j.applthermaleng.2011.05.045>.
  19. **Ramakrishna, D.; Basak, T.; Roy, S.; Momoniat, E.** 2014. Analysis of thermal efficiency via analysis of heat flow and entropy generation during natural convection within porous trapezoidal cavities, *International Journal of Heat and Mass Transfer* 77: 98-113.  
<https://doi.org/10.1016/j.ijheatmasstransfer.2014.04.002>.
  20. **Mahmoodi, M.** 2011. Numerical simulation of free convection of a nanofluid in L-shaped cavities, *International Journal of Thermal Sciences* 50(9): 1731-1740.  
<https://doi.org/10.1016/j.ijthermalsci.2011.04.009>.
  21. **Basak, T.; Aravind, G.; Roy, S.** 2009. Visualization of heat flow due to natural convection within triangular cavities using Bejan's heatline concept, *International Journal of Heat and Mass Transfer* 52(11-12): 2824-2833.  
<https://doi.org/10.1016/j.ijheatmasstransfer.2008.10.034>.
  22. **Asan, H.; Namli, L.** 2000. Laminar natural convection in a pitched roof of triangular cross-section: summer day boundary conditions, *Energy and Buildings* 33(1): 69-73.  
[https://doi.org/10.1016/S0378-7788\(00\)00066-9](https://doi.org/10.1016/S0378-7788(00)00066-9).
  23. **Akinsete, V. A.; Coleman, T. A.** 1982. Heat transfer by steady laminar free convection in triangular enclosures, *International Journal of Heat and Mass Transfer* 25(7): 991-998.  
[https://doi.org/10.1016/0017-9310\(82\)90074-6](https://doi.org/10.1016/0017-9310(82)90074-6).
  24. **Koca, A.; Oztop, H. F.; Varol, Y.** 2007. The effects of Prandtl number on natural convection in triangular enclosures with localized heating from below, *International Communications in Heat and Mass Transfer* 34(4): 511-519.  
<https://doi.org/10.1016/j.icheatmasstransfer.2007.01.006>.
  25. **Basak, T.; Roy, S.; Thirumalesha, C.** 2007. Finite element analysis of natural convection in a triangular enclosure: effects of various thermal boundary conditions, *Chemical Engineering Science* 62(9): 2623-2640.  
<https://doi.org/10.1016/j.ces.2007.01.053>.
  26. **Varol, Y.; Koca, A.; Oztop, H. F.** 2006. Natural convection in a triangle enclosure with flush mounted heater on the wall, *International Communications in Heat and Mass Transfer* 33(8): 951-958.  
<https://doi.org/10.1016/j.icheatmasstransfer.2006.05.003>.
  27. **Salmun, H.** 1995. Convection patterns in a triangular domain, *International Journal of Heat and Mass Transfer* 38(2): 351-362.  
[https://doi.org/10.1016/0017-9310\(95\)90029-2](https://doi.org/10.1016/0017-9310(95)90029-2).
  28. **Ben Nasr, K., Chouikh, R., Kerkeni, C., Guizani, A.** 2006. Numerical study of the natural convection in cavity heated from the lower corner and cooled from the ceiling, *Applied Thermal Engineering* 26(7): 772-775.  
<https://doi.org/10.1016/j.applthermaleng.2005.09.011>.
  29. **Hasanuzzaman, M.; Rahman, M. M.; Öztop, H. F.; Rahim, N. A.; Saidur, R.** 2012. Effects of Lewis number on heat and mass transfer in a triangular cavity, *International Communications in Heat and Mass Transfer* 39(8): 1213-1219.  
<https://doi.org/10.1016/j.icheatmasstransfer.2012.07.002>.
  30. **Kent, E. F.** 2009. Numerical analysis of laminar natural convection in isosceles triangular enclosures for cold base and hot inclined walls, *Mechanics Research Communications* 36(4): 497-508.  
<https://doi.org/10.1016/j.mechrescom.2008.11.002>.
  31. **Kaluri, R. S.; Anandalakshmi, R.; Basak, T.** 2010. Bejan's heatline analysis of natural convection in right-angled triangular enclosures: effects of aspect-ratio and thermal boundary conditions, *International Journal of Thermal Sciences* 49(9): 1576-1592.  
<https://doi.org/10.1016/j.ijthermalsci.2010.04.022>.
  32. **Tzeng, S. C.; Liou, J. H.; Jou, R. Y.** 2005. Numerical simulation-aided parametric analysis of natural convection in a roof of triangular enclosures, *Heat Transfer Engineering* 26(8): 69-79.  
<https://doi.org/10.1080/01457630591003899>.
  33. **Akinsete, V. A.; Coleman, T. A.** 1982. Heat transfer by steady laminar free convection in triangular enclosures, *International Journal of Heat and Mass Transfer* 25(7): 991-998.  
[https://doi.org/10.1016/0017-9310\(82\)90074-6](https://doi.org/10.1016/0017-9310(82)90074-6).
  34. **Kleszcz, S.; Mazur, P.; Zych, M.; Jaszczur, M.** 2022. An experimental investigation of the thermal efficiency and pressure drop for counterflow heat exchangers intended for recuperator, In *EPJ Web of Conferences* Vol. 269: 01027.  
<https://doi.org/10.1051/epjconf/202226901027>.
  35. **Ghouizi, J.; Nabou, M.; Elmir, M.; Douha, M.; Ber-ramdane, M.** 2020. Numerical simulation of natural convection in a cavity filled with a nanofluid whose wall containing the heat source is inclined, *Journal of Advanced Research in Fluid Mechanics and Thermal Sciences* 76(1): 1-16.  
<https://doi.org/10.37934/arfmts.76.1.116>.
  36. **Mosorov, V.; Zych, M.; Hanus, R.; Sankowski, D.; Saoud, A.** 2020. Improvement of flow velocity measurement algorithms based on correlation function and twin plane electrical capacitance tomography, *Sensors* 20(1): 306.  
<https://doi.org/10.3390/s20010306>.

E. Benachour, K. Asnoune, M. Hasnat, B. Draoui

#### UNSTEADY NUMERICAL INVESTIGATION STRATEGY OF NATURAL CONVECTION IN AN ISOSCELES SUPERIMPOSED TRIANGULAR ENCLOSURE

#### S u m m a r y

In power applications, convection plays a dominant position in the transport of strength for the proper design to attain higher warmth transfer quotes. Where in the fluid movement is genuinely induced via density gradients. This has a look at what is involved with transient convection in an isosceles-superimposed triangular enclo-

sure. The walls were angled at  $\theta = 45^\circ$ . Critical Rayleigh numbers have been obtained:  $Ra = 10^6$ , especially for the fluid crushed between the two triangles where we can visualize the critical convection transaction between the air and water. The consequences in the quantitative dimension of average Nusselt quantity change and qualitative visualization of streamline and isotherms are examined. The air and water streamlines and the temperature fields had been obtained for the Rayleigh numbers  $10^3 \leq Ra \leq 10^8$ . Furthermore, the water fluid's natural convection case has the best heat transfer performance at the water fluid, whereas the dilatant fluid exhibits the lowest heat transfer perfor-

mance. Heat transfer from the bottom to the top can be significantly improved by the triangle shape at first in a smooth and harmonious manner, and then it turns into a more complex and disorderly shape when the water reaches high temperatures.

**Keywords:** energy transfer, triangular enclosure, natural convection, heat transfer, triangular cavity.

Received May 4, 2023

Accepted February 15, 2024



This article is an Open Access article distributed under the terms and conditions of the Creative Commons Attribution 4.0 (CC BY 4.0) License (<http://creativecommons.org/licenses/by/4.0/>).